Journal on Electronic and Automation Engineering

Vol: 4(2), June 2025

REST Publisher; ISSN: 2583-6951 (Online)

Website: https://restpublisher.com/journals/jeae/

DOI: https://doi.org/10.46632/jeae/4/2/59

A New Multiport DC-DC Converter for DC Microgrid Applications

*** Yasa Uday Ranjan Reddy, K. Sowjanya, N. Madhukar Reddy**

Siddhartha Institute of Technology and Sciences, Korremula, Hyderabad, Telangana, India.

Corresponding author: **udaynmrec@gmail.com*

Abstract: *In this paper, a new multiport DC-DC converter is proposed for DC microgrid applications. Besides, the proposed configuration has several benefits for the design and operation of DC microgrids such as reducing multiple power conversions, reducing number of elements and voltage boosting capability. The bidirectional buck-boost structure of the proposed topology allows for enhanced flexibility to connect sources and loads with different voltage and power levels. The control strategy is developed to achieve power control for renewable sources such as MPPT for PV, in addition to a certain degree of resilience for DC sources availability while maintaining boosted DC link voltage. The key feature of the proposed configuration is that it offers full control over DC link voltage regardless of resource availability. A detailed steady state analysis is conducted to derive the voltage relations between all ports. Additionally, the state-space averaging followed by small-signal modelling and frequency response-based controller design for the proposed topology is discussed. A MATLAB/Simulink-based simulation study is conducted to demonstrate the performance of the proposed multiport converter topology under different operating conditions. Finally, the performance of the proposed multiport converter is validated through an experimental study.*

Keywords: *Battery, multiport converter, DC microgrid, photovoltaic, fuel cell*

1. INTRODUCTION

The transition of electrical grids toward decarbonization, decentralization, and digitalization has fueled growing interest in DC microgrids (DCMG) due to their higher reliability, efficiency, and simpler integration with renewable sources, energy storage, and DC loads compared to AC systems [1]. In a typical DCMG, multiple DC sources such as photovoltaic (PV) arrays, fuel cells (FC), and batteries are connected to a common DC bus through individual converters [2], enabling effective power management [3]. However, this architecture increases system cost, footprint, and complexity. To address this, multiport DC–DC converter topologies have been developed, classified into isolated [4]– [11] and non-isolated [12] [22] types. While isolated designs offer galvanic isolation and high voltage gain, they are bulky and complex. Non-isolated topologies are preferred for both islanded and grid-connected DCMGs due to their compact size and simpler control. This work focuses on non-isolated designs, proposing a new five-port converter interfacing PV, FC, and battery sources with two load ports.

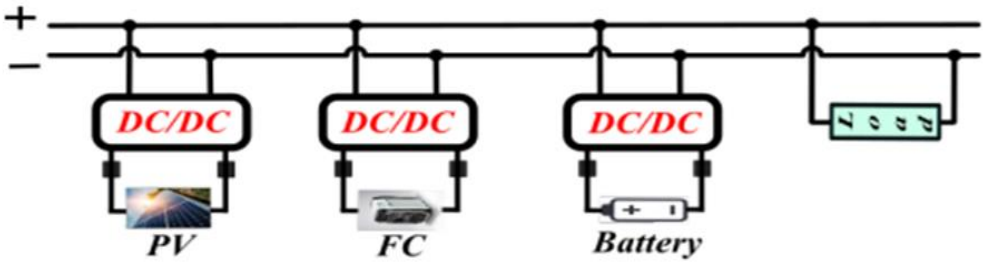

FIGURE 1. Typical DCMG Configuration

Existing non-isolated topologies, such as single-inductor multiple-output/multiple-input (SIMO) converters [12]–[14], reduce size and cost but suffer from cross-regulation issues. Other designs, like the single-inductor double-input double-output converter in [15], lack boosting capability, while the bipolar grid converter in [16] requires higher battery voltage than PV and uses many components. Similarly, the four-port topology in [17] and the buck–boost-based design in [18] reduce voltage stress or conversions but involve many components and limited bidirectionality. The bidirectional converter in [19] allows power flow in both directions but is bulky due to multiple inductors. Three-port converters (TPC) in [20] and [21] achieve high voltage gain and reduced component count but impose constraints on battery voltage and introduce high current ripple, affecting battery life. The topology in [22] reduces components and boosts DC link voltage but ties the link voltage to PV and battery levels, limiting independent regulation and requiring an additional boost stage for higher voltages.

TABLE 1. Comparison of Proposed Topology with Other Four and Five Port Topologies

Ref	No. of Switches	No. of Diodes	No. of L & C	Switches Max Voltage stress	Voltage Gain	No. of Ports	Availability and other limitations
[14]	3	4	2 & 6	$S_1 : V_{FC}$, $S_4 : V_{C3}$, S_2 and $S_3 : V_{Bat}$	$V_{out} = D_1 V_1 + (D_2 - D_1) V_2$	5	Sources Availability (No restriction) but $V_1 > V_2 > V_3 > V_4$
[15]	2	3	1 & 3	$S_1 V_{in}$ $S_2 : V_o$	$V_1 = \frac{V_{in2} D_1 - V_T (1-D_2) + V_{in1} (1-D_1)}{D_2}$	4	Sources Availability (No restriction) but $V_{pv} > V_o > V_{bat}$ and $R_2 > R_1$
[16]	3	4	3 & 5	$S_1 : (V_0^+)/d_1$ $S_2 : V_{pv} - V_{bat}$ $S_3 : V_0^+$	$V_{o1} = \frac{d_1 [V_{bat} d_2 + V_{pv} (1-d_2)]}{1-d_1}$ $V_{o2} = -\frac{d_1 [V_{bat} d_2 + V_{pv} (1-d_2)]}{1-d_1}$	4	Sources Availability (No restriction) but $V_{bat} > V_{pv}$
[17]	4	2	2 & 3	$S_1 : \frac{(1-d_3) V_2)}{(1-d_3) V_2 + (1-d_1) V_1}$, $S_2 : \frac{(1-d_1) V_1)}{3(1-d_3) V_2 + 3(1-d_1) V_1}$ $S_3 : \frac{(1-d_1) V_1}{(1-d_3) V_2 + (1-d_1) V_1}$ $S_4 : \frac{(1-d_2) V_1)}{d_4 V_2 + (1-d_2) V_1}$	$V_o 1 = \frac{V_2}{1-d_2} + \frac{V_1}{d_4}$ $V_o 2 = \frac{V_1}{d_4}$	4	Both sources should be available
[22]	3	1	3 & 5	S_1, S_2 and $S_4 : V_o$	$V_o = V_{PV} + V_{bat}$	4	Sources Availability (No restriction) but $V_o = V_{bat} + V_{pv}$
Proposed	4	0	2 & 5	S_1 and S_2: $V_{pv} + V_{bat}$ S_3 and S_4: V_o	$V_o = \frac{1}{1-D_4} V_{FC} + \frac{1-D_1-2D_4}{(1-D_4} (V_{PV} + V_{bat})$	5	FC should be available no restriction for all sources voltages

To overcome these limitations, the proposed five-port non-isolated DC–DC converter [23] offers bidirectional buck–boost operation with flexible interfacing of three sources and two loads at different voltages and power levels. Key advantages include: (i) full control over DC link voltage independent of PV availability, (ii) reduced component count compared to similar literature, and (iii) a simple control strategy enabling PV MPPT and DC link regulation under all operating modes. The paper proceeds with steady-state analysis and operational modes (Section III), control strategy and small-signal modelling (Section III), simulation and experimental validation (Sections III and IV), and concludes with performance evaluation (Section V)

2. LITERATURE REVIEW

Research on DC microgrids has evolved substantially over the past decade, with a strong focus on control strategies, stabilization techniques, and multi-source integration. Dragicevic et al. [1] [2] provide comprehensive reviews of control methodologies for DC microgrids, addressing droop control, hierarchical control, and stabilization approaches essential for maintaining voltage regulation and load sharing. These works also highlight the importance of standardization and power architecture considerations in facilitating the deployment of microgrids across diverse applications. Lu et al. [26] further contribute by introducing a state-of-charge-based droop control method for distributed energy storage systems, enhancing energy balance in autonomous microgrids. Similarly, Tonkoski et al.

[28] discuss coordinated power curtailment techniques for PV inverters to mitigate overvoltage issues in grid-connected systems, underscoring the need for dynamic and adaptive control mechanisms. Parallel to advancements in control, significant research has been directed toward the development of multi-input, multi-output (MIMO) DC–DC converter topologies for hybrid energy systems. Early works, such as Chiu et al. [4] and Zhao et al. [5], explored multiple-input converters enabling integration of renewable energy sources with storage devices, while Tao et al. [6], [9] introduced transformer-coupled and triple-half-bridge designs for improved power flow management. Subsequent innovations expanded to four-port and reconfigurable topologies [15], [16], [21] that interface PV, fuel cells, and batteries with microgrids, providing high voltage gain and decoupled power flow control. Designs such as those by Kardan et al. [18], Nejabatkhah et al. [24], and Jalilzadeh et al. [17] specifically target hybrid PV/FC/battery configurations, optimizing voltage stress reduction and improving efficiency. The trend reflects a clear shift toward compact, flexible, and high-efficiency converter architectures suitable for both isolated and non-isolated applications. Control strategies for hybrid energy storage systems (HESS) and renewable integration have also been extensively studied to enhance reliability and power quality. Kollimalla et al. [3] proposed coordinated battery–supercapacitor management to handle dynamic load and source variations effectively. Akar et al. [19] designed a bidirectional multi-input converter for electric vehicle storage systems, enabling high-power bidirectional flow between batteries and ultracapacitors. Ravada et al. [22], [27] investigated multi-source converter configurations for PV-wind-HESS-based microgrids, achieving seamless transition between grid-interactive and autonomous modes. Prabhakaran and Agarwal [15] addressed low-voltage bipolar DC microgrid interfacing, while Wang et al. [10] and Krishnaswami and Mohan [11] contributed high-efficiency three-port converters for fuel cell vehicles and renewable integration. These developments, combined with MPPT algorithms such as perturb-and-observe [25], demonstrate a holistic research trend toward maximizing renewable penetration while ensuring stable, high-quality power delivery in both grid-connected and standalone microgrid environments.

3. PROPOSED METHODOLOGY

Maximum Power Point Tracking (MPPT) is an electronic system that optimizes the operating point of PV modules to extract maximum possible power. It differs from mechanical tracking, which physically moves panels to face the sun, though both can be used together. MPPT adjusts voltage or current electronically to achieve the maximum power point under varying temperature and irradiance. The extra harvested power is delivered as increased battery charging current. One common method, Fractional Open-Circuit Voltage, uses the nearly constant ratio of maximum power voltage (VMPP) to open-circuit voltage (VOC).

$$V_{MPP} \approx k_1 V_{OC}$$

This factor k1 has been reported to be between 0.71 and0.78. Once the constant k1 is known, VMPP is computed by measuring VOC periodically. Although the implementation of this method is simple and cheap, its tracking efficiency is relatively low due to the utilization of inaccurate values of the constant k1 in the computation of VMMP.

Fractional Short-Circuit Current

The method results from the fact that, the current at maximum power point IMPP is approximately linearly related to the short circuit current ISC of the PV array.

$$I_{MPP} \approx k_2 I_{SC}$$

Like in the fractional voltage method, k2 is not constant. It is found to be between 0.78 and 0.92. The accuracy of the method and tracking efficiency depends on the accuracy of K2and periodic measurement of short circuit current.

Perturb and Observe

The Perturb and Observe (P&O) MPPT method adjusts PV array voltage by incrementing or decrementing it based on output power changes from sampled voltage and current. If power increases, the next perturbation is in the same direction; if it decreases, the direction is reversed, causing oscillation around the MPP. Smaller perturbation steps

reduce oscillations but slow tracking, so variable step sizes are used; larger when far from MPP, smaller when near. The method struggles under rapidly changing atmospheric conditions. Improvements include three-point weight comparison and two-stage algorithms for faster and more precise tracking

Incremental Conductance

The method is based on the principle that the slope of the PV array power curve is zero at the maximum power point. (dP/dV) = 0. Since (P = VI), it yields:

$$\Delta I/\Delta V = -I/V \text{ , at MPP}$$
$$\Delta I/\Delta V > -I/V \text{ , left of MPP}$$
$$\Delta I/\Delta V < -I/V \text{ , right of MPP}$$

The Incremental Conductance (INC) MPPT method tracks MPP by comparing instantaneous conductance (I/V) with incremental conductance (ΔI/ΔV). The array reference voltage is adjusted until the two values matches, maintaining operation at MPP once reached. This method demands high sampling rates and fast slope calculations for accuracy. In contrast, conventional charge controllers connect PV modules directly to the battery, forcing them to operate at battery voltage. This voltage is usually below the ideal MPP voltage, limiting power output. For example, a 75 W module forced to operate at 12 V produces only about 53 W instead of its maximum capacity.

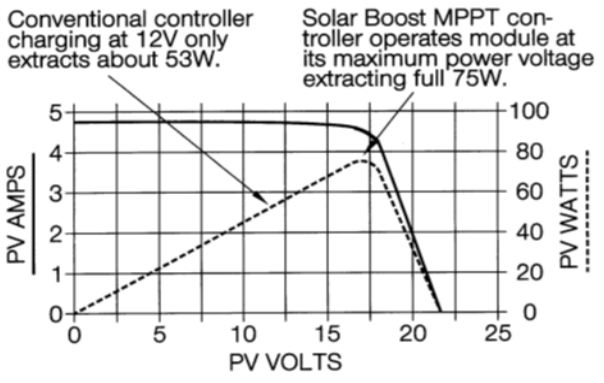

FIGURE 2.

The patented MPPT system in a Solar Boost charge controller optimizes power extraction by operating the PV module at its maximum power voltage (VMP), such as 17V, instead of simply connecting it to the battery voltage (e.g., 12V). This allows the controller's high-efficiency DC-DC converter to boost the module voltage to match the battery voltage, increasing the charge current—potentially by 42% in ideal conditions—compared to conventional controllers that limit power output. Although real-world inefficiencies reduce this gain, the charge current increase depends on factors like the difference between VMP and battery voltage, PV module temperature (cooler temperatures raise VMP), and battery state of charge, with highly discharged batteries enabling higher current due to lower voltage, effectively delivering nearly constant power to the battery.

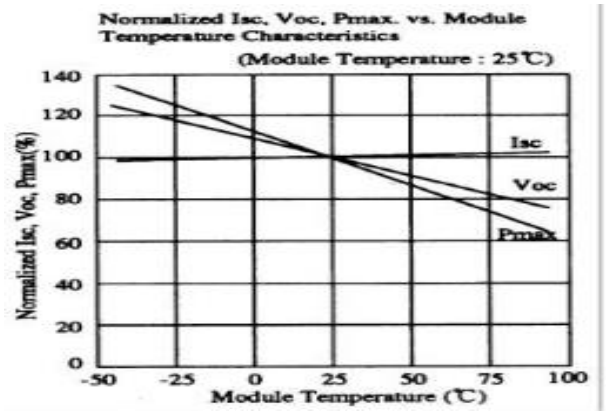

FIGURE 3.

Fuel cell systems operating on air experience efficiency losses due to air pressurization and dehumidification, bringing their efficiency close to that of compression ignition engines, and fuel cell efficiency decreases with increasing load. While fuel cell vehicles can achieve tank-to-wheel efficiencies above 45% at low loads and around 36% under driving cycles like the NEDC—compared to about 22% for diesel vehicles—overall efficiency from hydrogen production to wheel is lower, especially considering energy losses in fuel production, storage, and distribution. Unlike batteries, fuel cells cannot store energy but can be combined with electrolyzes for long-term hydrogen storage, though round-trip efficiency remains between 30-50%. High-temperature solid-oxide fuel cells can capture waste heat to reach total efficiencies of 80-90% in combined heat and power applications. Stationary fuel cells serve as grid-connected or independent power sources, with specific codes and standards guiding their installation. The proposed multiport DC-DC converter topology connects three DC sources—PV, fuel cell, and battery—and two loads with only four IGBT switches, enabling PV MPPT, battery charge/discharge, and DC link voltage regulation even without PV availability, using inductors and capacitors for power buffering and energy transfer across ports.

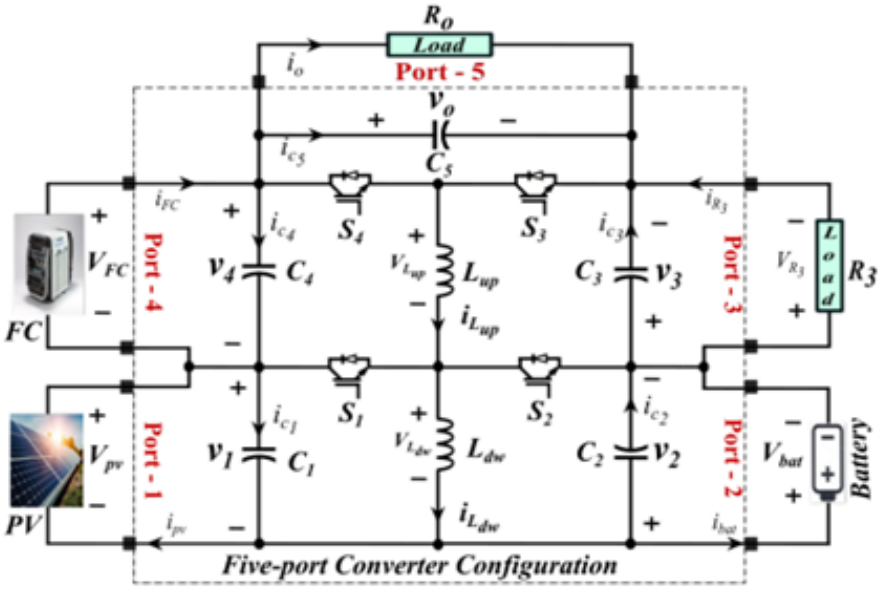

FIGURE 4. Proposed multiport DC-DC converter.

Modes Of Operation

Fuel cell systems face efficiency losses from air pressurization and dehumidification, with efficiency decreasing at higher loads, yet still achieving better tank-to-wheel efficiencies than diesel vehicles. Unlike batteries, fuel cells cannot store energy but can be paired with electrolyzers for hydrogen storage, with round-trip efficiencies of 30-50%. High-temperature solid-oxide fuel cells capture waste heat to boost total efficiency in combined heat and power applications. Stationary fuel cells serve both grid-connected and off-grid roles, governed by specific standards.

$$S1 = S^{-}2 \ (d1)$$

$$S4 = S^{-}3 \ (d4)$$

The proposed multiport DC-DC converter connects PV, fuel cell, and battery sources to two loads using four IGBT switches, enabling independent control of upper and lower ports through variable duty cycles d4 and d1, respectively. When PV is available, d1 controls MPPT via a perturb and observe method; otherwise, it manages battery power. Operating scenarios based on duty cycle comparisons (d1 > d4, d4 > d1, d1 = d4) define switching states that manage energy flow among sources and loads. For example, when PV power exceeds load demand, excess energy charges the battery, and when demand exceeds generation, the battery discharges to support loads. Detailed switching sequences govern the charging and discharging of inductors and energy transfer across ports to maintain the desired DC link voltage and maximize efficiency.

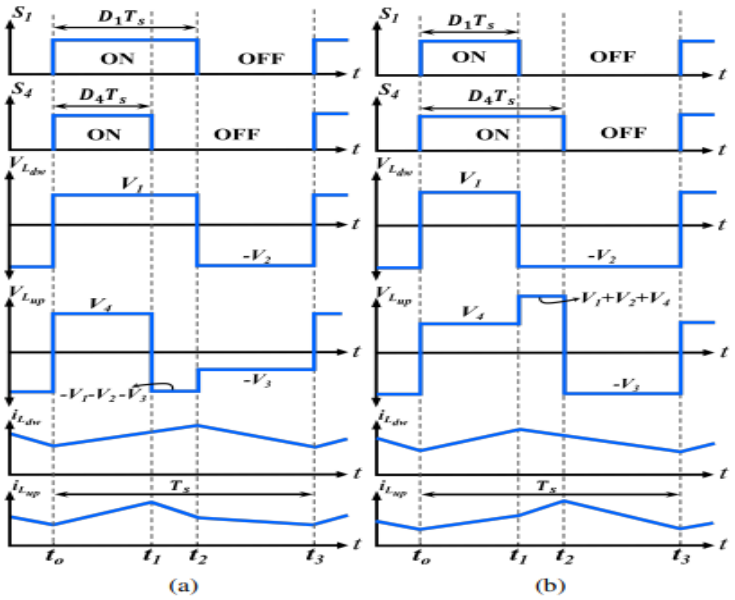

FIGURE 5. Switching states and inductors voltages and currents in different cases: (a) D1Ts > D4Ts, (b) D4Ts > D1Ts

Steady State Analysis

Typically for all modes of operation, as S1 and S2 are driven complementary, by applying volt-second balance across the L_{dw} inductor, the relation between PV and battery ports is the same as the bidirectional buck-boost DC-DC converter:

$$\frac{V_2}{V_1} = \frac{V_{bat}}{V_{pv}} = \frac{D_1}{1 - D_1}$$

Applying volt-second balance on L_{up} to obtain the voltage gain for port-3 (in case D1Ts > D4Ts) as in figure:

$$V4D4Ts + (-V3 - V1 - V2)\,(D1 - D4)\,Ts - V3\,(1 - D1)\,Ts = 0$$

Rearranging to determine port-3 voltage in terms of other voltages,

$$V_3 = \frac{D_4}{1 - D_4} V_4 + \frac{D_1 - D_4}{1 - D_4}\,(V_1 + V_2)$$

$$V_3 = \frac{D_4}{1 - D_4} V_{FC} + \frac{D_1 - D_4}{1 - D_4}\,(V_{PV} + V_{bat})$$

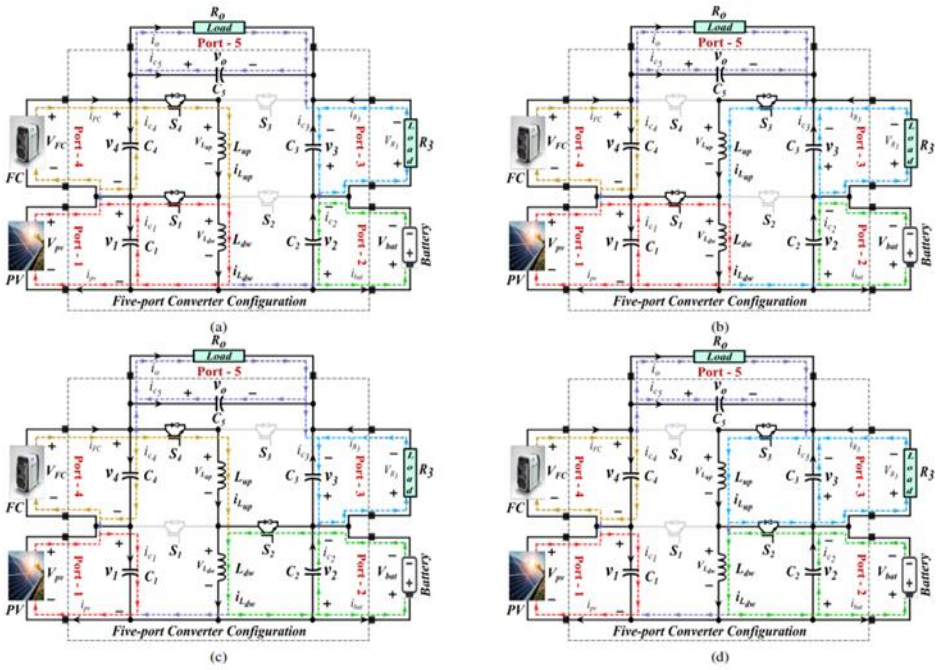

FIGURE 6. Mode I: PV and FC are available with d1 > d4: (a) S1 and S4 are ON, (b) S1 and S3 are ON, (c) S2 and S4 are ON and (d) S3 and S4 are ON

Applying volt-second balance on L_{up} to determine the voltage gain for port 3 (in case D4Ts > D1Ts as shown in figure:

$$V_3 = \frac{D_4}{1-D_4}V_4 + \frac{D_4 - D_1}{1-D_4}\ (V_1 + V_2)$$

$$V_3 = \frac{D_4}{1-D_4}V_{FC} + \frac{D_4 - D_1}{1-D_4}\ (V_{PV} + V_{bat})$$

The DC link voltage is the sum of all other ports voltages and can be expressed as follows:

$$V_o = V_1 + V_2 + V_4 + V_3$$

$$V_o = V_{PV} + V_{bat} + V_{FC} + V_{R_3}$$

By substituting equation (6) in equation (10), the output voltage can be expressed as:

$$V_o = \frac{1}{1-D_4}V_{FC} + \frac{1 - D_1 - 2D_4}{1-D_4}\ (V_{PV} + V_{bat})$$

By substituting equation (8) in equation (10), the output voltage can be expressed as:

$$V_o = \frac{1}{1-D_4}V_{FC} + \frac{1 - D_1}{1-D_4}\ (V_{PV} + V_{bat})$$

Comparison with previous work

A detailed comparison in Table-I shows that the proposed topology uses fewer components (11 vs. 15) than the five-port topology in [14], with no restrictions on source interfacing unlike [14] and [15]. It also achieves higher voltage gain without duty cycle limitations compared to prior designs. These improvements enhance flexibility and efficiency in DC microgrid applications [14], [15].

4. DYNAMIC MODELING AND CONTROLLER DESIGN OF THE PROPOSED MULTIPORT CONVERTER

In this section, the dynamic linearized model of the proposed multiport converter is derived through state-space averaging followed by small signal modelling.

A. Dynamic Modelling

The proposed topology includes five capacitors and two inductors, forming a seven-order system with six state variables and two control inputs. The fifth port voltage is estimated by summing other port voltages, simplifying it to a six-order system. The main control goals are regulating the DC link voltage, achieving MPPT in Mode-I, and controlling battery power in Mode-II. Out of the six states, four outputs—iLdw, iLup, v1, and vo—are controlled to meet these objectives. The state-space averaged d1>d2 in this system.

$$L_{dw}\frac{di_{L_{dw}}}{dt} = v_1 d_1 - (1-d_1)\,v_2$$

$$L_{up}\frac{di_{L_{up}}}{dt} = v_4 d_3 - (v_1+v_2)\,(d_1-d_4) - v_3\,(1-d_4)$$

$$C_1\frac{dv_1}{dt} = i_{pv} - \frac{v_o}{R_o} - i_{L_{dw}} d_1 + i_{L_{up}}\,(d_1-d_4)$$

$$C_2\frac{dv_2}{dt} = i_{L_{dw}}\,(1-d_1) + i_{L_{up}}\,(d_1-d_4) - i_{bat} - \frac{v_o}{R_o}$$

$$C_3\frac{dv_3}{dt} = i_{L_{up}}\,(1-d_4) - \frac{v_3}{R_3} - \frac{v_o}{R_o}$$

$$C_4\frac{dv_4}{dt} = i_{FC} - \frac{v_o}{R_o} - i_{L_{up}} d_4$$

In mode-I, when d4 > d1, all above equations are the same. In case where PV is not available in mode-II, the previous dynamic model equations for both d1 ≥ d4 and d4 > d1 are valid taking into consideration ipv = 0. The nonlinear model of the proposed converter is linearized around the equilibrium point using small signal modelling as explained in [24] as follow,

x = X + xe; u = U + u and w e = W +

were,

$$x = \begin{bmatrix} i_{L_{dw}} \\ i_{L_{up}} \\ v_1 \\ v_2 \\ v_3 \\ v_4 \end{bmatrix}, u = \begin{bmatrix} d_1 \\ d_4 \end{bmatrix} \quad and \quad w = \begin{bmatrix} i_{pv} \\ i_{bat} \\ i_{FC} \end{bmatrix}$$

x is the state vector, u is the input vector and w is the disturbance vector. By substituting (19) in each mode model and ignoring higher order terms, the linear small-signal model of the proposed topology in all modes of operation as follow:

$$\left.\begin{aligned}\dot{\tilde{x}} &= A\,\tilde{x} + B\,\tilde{u} + E\,\tilde{w}\\ \tilde{y} &= C\,\tilde{x}\end{aligned}\right\}$$

In state and output equation (21), xe ,ue , we and ye are the state vector, input control vector, disturbance variable vector and output vector respectively which are defined as:

$$\tilde{x} = \begin{bmatrix}\tilde{i}_{L_{dw}}\\ \tilde{i}_{L_{up}}\\ \tilde{v}_1\\ \tilde{v}_2\\ \tilde{v}_3\\ \tilde{v}_4\end{bmatrix}, \tilde{u} = \begin{bmatrix}\tilde{d}_1\\ \tilde{d}_4\end{bmatrix}, \tilde{w} = \begin{bmatrix}\tilde{i}_{pv}\\ \tilde{i}_{bat}\\ \tilde{i}_{FC}\end{bmatrix}, and\ \ y = \begin{bmatrix}\tilde{i}_{L_{dw}}\\ \tilde{i}_{L_{up}}\\ \tilde{v}_1\\ \tilde{v}_o\end{bmatrix}$$

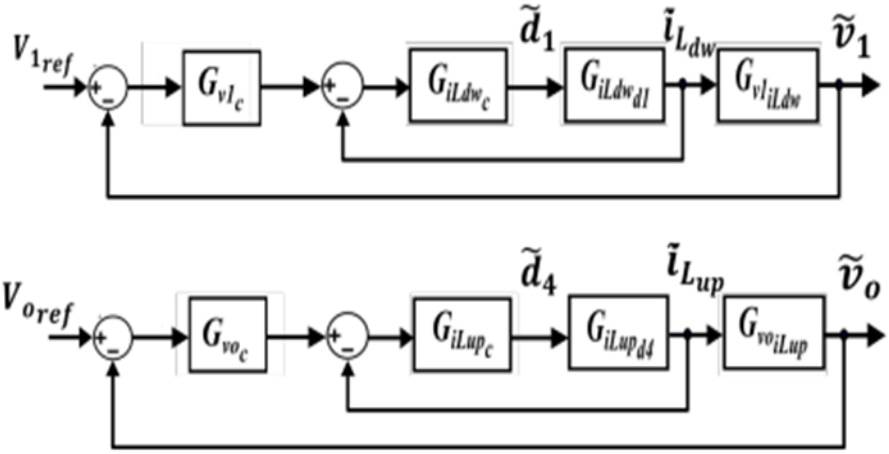

FIGURE 7. Dual Loop Control Block Diagram for the Proposed Converter.

The A, B, E and C matrices change depending on the operating modes of the proposed converter. The output matrix C is the same for all modes and it is given as follows:

$$C = \begin{bmatrix}1 & 0 & 0 & 0 & 0 & 0\\ 0 & 1 & 0 & 0 & 0 & 0\\ 0 & 0 & 1 & 0 & 0 & 0\\ 0 & 0 & 1 & 1 & 1 & 1\end{bmatrix}$$

The state-space matrices for Mode-I with d1 ≥ d4 are given below:

$$A = \begin{bmatrix} 0 & 0 & \frac{D_1}{L_{dw}} & \frac{D_1-1}{L_{dw}} & 0 & 0 \\ 0 & 0 & \frac{D_4-D_1}{L_{up}} & \frac{D_4-D_1}{L_{up}} & \frac{D_4-1}{L_{up}} & \frac{D_4}{L_{up}} \\ \frac{-D_1}{C_1} & \frac{D_1-D_4}{C_1} & \frac{-1}{C_1R_o} & \frac{-1}{C_1R_o} & \frac{-1}{C_1R_o} & \frac{-1}{C_1R_o} \\ \frac{1-D_1}{C_2} & \frac{D_1-D_4}{C_2} & \frac{-1}{C_2R_o} & \frac{-1}{C_2R_o} & \frac{-1}{C_2R_o} & \frac{-1}{C_2R_o} \\ 0 & \frac{(1-D_4)}{C_3} & \frac{-1}{C_3R_o} & \frac{-1}{C_3R_o} & \frac{-1}{C_3R_o} - \frac{1}{C_3R_3} & \frac{-1}{C_3R_o} \\ 0 & \frac{-D_4}{C_4} & \frac{-1}{C_4R_o} & \frac{-1}{C_4R_o} & \frac{-1}{C_4R_o} & \frac{-1}{C_4R_o} \end{bmatrix} \quad (24)$$

$$B = \begin{bmatrix} \frac{V_1+V_2}{L_{dw}} & 0 \\ -\frac{(V_1+V_2)}{L_{up}} & \frac{V_1+V_2+V_3+V_4}{L_{up}} \\ \frac{I_{Lup}-I_{Ldw}}{C_1} & -\frac{I_{Lup}}{C_1} \\ \frac{I_{Lup}-I_{Ldw}}{C_2} & -\frac{I_{Lup}}{C_2} \\ 0 & -\frac{I_{Lup}}{C_3} \\ 0 & -\frac{I_{Lup}}{C_4} \end{bmatrix}, E = \begin{bmatrix} 0 & 0 & 0 \\ 0 & 0 & 0 \\ \frac{1}{C_1} & 0 & 0 \\ 0 & -\frac{1}{C_2} & 0 \\ 0 & 0 & 0 \\ 0 & 0 & \frac{1}{C_4} \end{bmatrix}$$

Finally, the transfer matrices between inputs, disturbances and output could be obtained by applying the Laplace transform to (21) employing the following equations:

$$G_{y\tilde{u}}(s) = C[sI - A]^{-1} B$$

$$T_{y\tilde{w}}(s) = C[sI - A]^{-1} E$$

Where, Gyue (s) is the transfer matrix relating output vector states eiLdw, eiLup, ve1 and veo with both control inputs de1 and de4. On the other hand, Tywe (s) is the transfer matrix relating output vector states with disturbance vector states eipv, eibat and eiFC.

Controller Design

As discussed in the previous sections, the proposed converter has two pairs of switches driven in a complementary way using two separate duty cycles acting as two control input. The duty cycle d1 controls switch pair S1 − S2 which in turn controls inductor Ldw current to regulate the power flow between Port1 and Port-2. Similarly, the duty cycle d4 controls switch pair S3 − S4 to regulate the DC link load voltage through inductor.

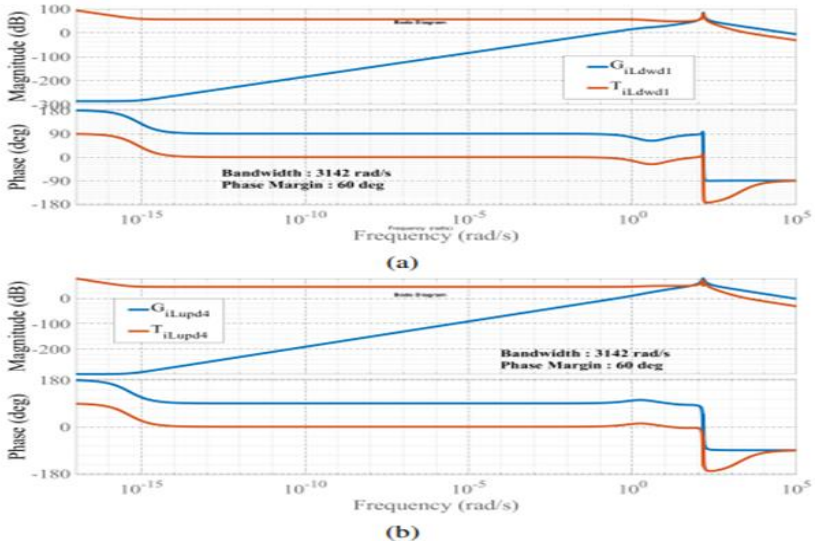

FIGURE 8. Frequency response inner current loops with and without controller: (a) inductor Ldw current loop and (b) inductor Lup current loop.

L_{up}. further, as explained in the modelling section, the proposed converter system has several couplings, hence the cascaded dual loop control is considered for the controller design procedures. Thus, two cascaded dual loops are used, first to control current iL_{dw} and Port-1 voltage v1 (as MPPT control when PV is available or battery power drooped control when PV is not available). The second cascaded dual loop regulates current iL_{up} and load DC link voltage vo. Based on these objectives, using (26), the transfer functions for lower two-ports can be represented as,

$$G_{iLdw_{d1}}(s) = G_{y\tilde{u}_{(1,1)}}(s) = \frac{\tilde{i}_{L_{dw}}(s)}{\tilde{d}_1(s)}$$

$$G_{v_{1\,iLdw}}(s) = \frac{G_{y\tilde{u}_{(1,1)}}(s)}{G_{y\tilde{u}_{(3,1)}}(s)} = \frac{\tilde{v}_1(s)}{\tilde{i}_{Ldw}(s)}$$

where, GiLdwd1 (s) represents the open loop transfer function between inductor Ldw current (eiLdw) and duty cycle (de1). Furthermore, the open loop transfer function between Port-1 voltage (ve1) to inductor Ldw current is got by Gv1iLdw (s). Similarly, using (26) the transfer functions for upper two-ports can be expressed as follow,

$$G_{iLup_{d4}}(s) = G_{y\tilde{u}_{(2,2)}}(s) = \frac{\tilde{i}_{Lup}(s)}{\tilde{d}_4(s)}$$

$$G_{v_{o\,iLup}}(s) = \frac{G_{y\tilde{u}_{(2,2)}}(s)}{G_{y\tilde{u}_{(4,2)}}(s)} = \frac{\tilde{v}_o(s)}{\tilde{i}_{Lup}(s)}$$

Where, GiLupd4 (s) represents the open loop transfer function between inductor Lup current (eiLup) and duty cycle (de4). On the other hand, the open loop transfer function between DC link load voltage (veo) to inductor Lup current is got by GvoiLup (s). The overall control diagram for the proposed multiport topology using (a) (b)

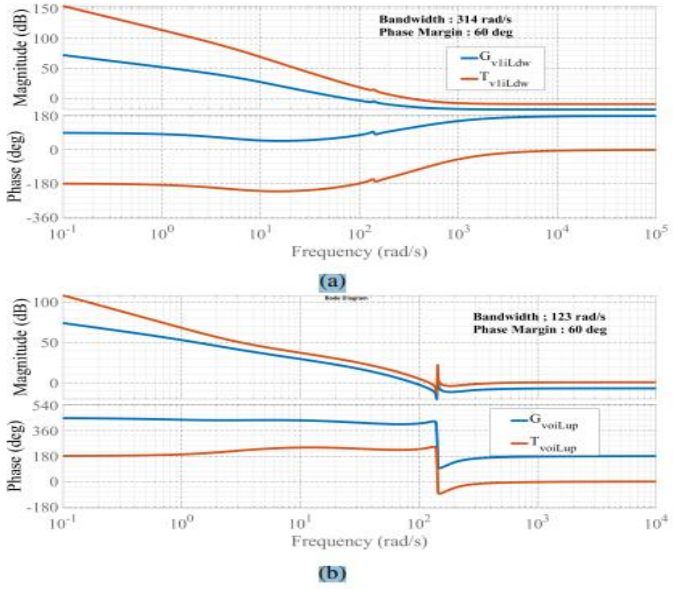

FIGURE 9. Frequency Response Outer Voltage Loops with and without Controller: (a) Port-1 voltage (ve1) loop and (b) DC link load voltage (veo) loop.

(28)-(31) is shown in figure. As the converter system is a six-order system, MATLAB control toolbox (SISO Tool) is utilized to determine the transfer functions and the controller designed parameters. The proportional- integral (PI) controllers are used to control inductor currents and port voltages as per below: The control parameters are designed considering the switching frequency as 5 kHz and the bandwidth of the current controllers is chosen to be 1/10th of the switching frequency, that is, 3.142 krad/s with a phase margin 60o. Based on this, KpiLdw, KiiLdw , KpiLup and KiiLup are computed as 0.055, 101.16, 0.034 and 61.7, respectively, for the inner two current control loops. For the outer voltage loops, the bandwidth of v1 loop is chosen to be 314 rad/s with proportional gain Kpv1 = 2.861 and integral gain Kiv1 = 1244, whereas vo loop has 123 rad/s as bandwidth, hence Kpvo = 2.36 and Kivo = 5.14. Using these parameters, the frequency responses for the inner current loops with and without compensations are given in Fig. 6. The frequency responses for the outer voltage loops are provided in Fig. 3.6. It can be noticed that both the current controller loop bandwidths are around 3.142krad/s and for the voltage control loops are 314 rad/s and 123 rad/s with a phase margin of 60o.

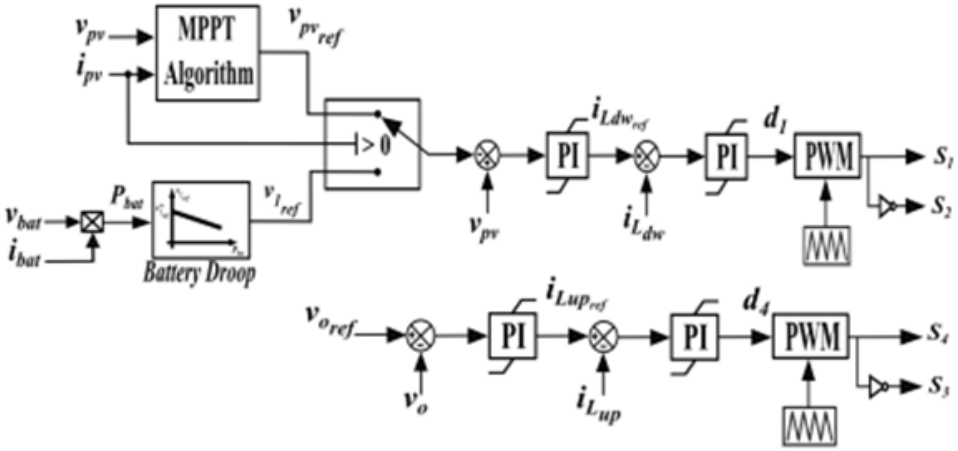

FIGURE 10. Control Structure of the Proposed Topology.

C. Overall Control Scheme

The control strategy for the proposed converter (Fig. 8) uses inner loops regulating inductor currents and capacitor voltages via cascaded PI controllers in the zero-control layer. This layer receives commands from the primary control layer, which implements MPPT using the perturb and observe (P&O) method [25] in Mode-I or battery droop control in Mode-II. The P&O algorithm measures PV voltage and current at intervals to calculate power variations, adjusting voltage perturbations accordingly. When PV is unavailable (Mode-II), battery power is controlled through DC droop based on capacitor voltage v1 [26]. This approach ensures efficient power management under varying conditions.

$$V1ref = V * 1ref - mPbat$$

The battery average power PbatP_{bat}Pbat and droop coefficient mmm determine the reference voltage V1ref∗V_{1ref} ^*V1ref∗, with mmm based on battery state of charge (SoC) estimation as per [26], [27]. In Mode-I, when PV power exceeds load and the battery is fully charged (SoC at 100%), the system switches to power curtailment, disabling MPPT to protect the battery [28]. This ensures safe battery operation under high PV generation.

5. RESULTS AND DISCUSSION

A MATLAB/Simulink simulation model was developed to evaluate the proposed multiport converter for DC microgrid applications using parameters such as PV source (VpvMPP_{pvMPP}pvMPP = 54.7 V, IpvMPP_{pvMPP}pvMPP = 5.98 A), fuel cell (VFCrated_{FCrated}FCrated = 36 V, IFCrated_{FCrated}FCrated = 8.3 A), and battery (51.2 V, 25 Ah). In Mode-I, with PV available, the system tracked the maximum power point while maintaining the DC link voltage at 220 V. The PV generated 327 W, and the fuel cell supplied 142.2 W to the loads, with surplus power charging the battery. When loads increased, the fuel cell and battery adjusted power supply accordingly, and the DC link voltage remained stable even when solar irradiance dropped by half. This flexible DC link voltage regulation surpasses previous converters such as [22]. In Mode-II, without PV availability, the battery

and fuel cell together supplied the loads while maintaining the DC link voltage at 220 V. As the Port-3 and DC link loads increased, both battery discharge and fuel cell output power rose to meet demand. The PV and battery voltages remained constant, but the fuel cell output voltage varied slightly with power changes, which in turn affected the Port-3 voltage. The simulation results demonstrated that the proposed converter effectively regulates DC link voltage and shares power among sources under varying load conditions and source availability [23].

TABLE 2. System Parameters used for Experimental Validation

Parameter	Value
Photovoltaic source	Agilent E4350B Solar Array Simulator
Fuel Cell source	Chroma programmable power supply
Two lithium batteries	$V_{bat\,rated} = 60V$ Nominal Capacity = 5 Ah
Four Port Converter	$C_1 = C_2 = C_4 = 2.2\ mF$ $C_3 = C_5 = 1.26\ mF;\ L_{dw} = L_{up} = 2.6\ mH$ Two SMK 50GB123D IGBT Modules
Electronic Load	$R_o = (110 - 220)\ \Omega$ (250W−500W)
Controller	150 MHz Texas Instrument digital signal controller (TMS320F28335)

6. CONCLUSION AND FUTURE SCOPE

In this paper, a new multiport DC-DC converter for DC microgrid applications has been presented. Three sources with two loads are interfaced to the proposed converter with minimum possible elements reducing power losses and system size. The bidirectional buck-boost structure of this new topology has shown a significant flexibility to connect sources and loads with different voltage and power levels. The control strategy is developed to achieve power control for renewable sources such as PV MPPT, in addition to a certain degree of resilience for DC sources availability maintaining boosted DC link voltage. The DC link voltage is strictly regulated in all operating modes proving that the proposed architecture has a substantial relevance among other configurations previously developed in the literature. The proposed converter's effectiveness and performance are evaluated and verified through both simulation and experimental results under different modes of operation.

REFERENCES

[1]. T. Dragovic, X. Lu, J. C. Vasquez and J. M. Guerrero," DC Microgrids—Part ´ I: A Review of Control Strategies and Stabilization Techniques," in IEEE Transactions on Power Electronics, vol. 31, no. 7, pp. 4876-4891, July 2016.

[2]. T. Dragicevi ˇ c, X. Lu, J. C. Vasquez and J. M. Guerrero," DC Micro- ´ grids—Part II: A Review of Power Architectures, Applications, and Standardization Issues," in IEEE Transactions on Power Electronics, vol. 31, no. 5, pp. 3528-3549, May 2016.

[3]. S. K. Kollimalla, M. K. Mishra and N. L. Narasamma," Design and Analysisof Novel Control Strategy for Battery and Supercapacitor Storage System," in IEEE Transactions on Sustainable Energy, vol. 5, no. 4, pp. 1137-1144, Oct. 2014.

[4]. Huang-Jen Chiu, Hsiu-Ming Huang, Li-Wei Lin and Ming-Hsiang Tseng," A multiple-input DC/DC converter for renewable energy systems," 2005 IEEE International Conference on Industrial Technology, 2005, pp. 1304- 1308, doi: 10.1109/ICIT.2005.1600837.

[5]. C. Zhao, S. D. Round and J. W. Kolar," An Isolated Three-Port Bidirectional DC-DC Converter with Decoupled Power Flow Management," in IEEE Transactions on Power Electronics, vol. 23, no. 5, pp. 2443-2453, Sept. 2008, doi: 10.1109/TPEL.2008.2002056.

[6]. H. Tao, A. Kotsopoulos, J. L. Duarte and M. A. M. Hendrix," TransformerCoupled Multiport ZVS Bidirectional DC–DC Converter with Wide Input Range," in IEEE Transactions on Power Electronics, vol. 23, no. 2, pp. 771-781, March 2008, doi: 10.1109/TPEL.2007.915129.

[7]. B. Mangu, S. Akshatha, D. Suryanarayana and B. G. Fernandes," GridConnected PV-Wind-Battery-Based Multi-Input Transformer-Coupled Bidirectional DC-DC Converter for Household Applications," in IEEE Journal of Emerging and Selected Topics in Power Electronics, vol. 4, no. 3, pp. 1086-1095, Sept. 2016, doi: 10.1109/JESTPE.2016.2544789.

[8]. J. Deng, H. Wang and M. Shang," A ZVS Three-Port DC/DC Converter for High-Voltage Bus-Based Photovoltaic Systems," in IEEE Transactions on Power Electronics, vol. 34, no. 11, pp. 10688-10699, Nov. 2019, doi: 10.1109/TPEL.2019.2895976.
[9]. Haimin Tao, A. Kotsopoulos, J. L. Duarte and M. A. M. Hendrix," Triple-half-bridge bidirectional converter controlled by phase shift and PWM," Twenty-First Annual IEEE Applied Power Electronics Conference and Exposition, 2006. APEC '06., 2006, pp. 7 pp.-, doi: 10.1109/APEC.2006.1620700.
[10]. L. Wang, Z. Wang and H. Li," Asymmetrical Duty Cycle Control and Decoupled Power Flow Design of a Three-port Bidirectional DC-DC Converter for Fuel Cell Vehicle Application," in IEEE Transactions on Power Electronics, vol. 27, no. 2, pp. 891-904, Feb. 2012, doi: 10.1109/TPEL.2011.2160405.
[11]. H. Krishnaswami and N. Mohan," Three-Port Series-Resonant DC–DC Converter to Interface Renewable Energy Sources with Bidirectional Load and Energy Storage Ports," in IEEE Transactions on Power Electronics, vol. 24, no. 10, pp. 2289-2297, Oct. 2009, doi: 10.1109/TPEL.2009.2022756.
[12]. H. Behjati and A. Davoudi," A Multiple-Input Multiple-Output DC–DC Converter," in IEEE Transactions on Industry Applications, vol. 49, no. 3, pp. 1464-1479, May-June 2013.
[13]. G. Chen, Y. Liu, X. Qing, M. Ma and Z. Lin," Principle and Topology Derivation of Single-Inductor Multi-Input Multi-Output DC–DC Converters," in IEEE Transactions on Industrial Electronics, vol. 68, no. 1, pp. 25-36, Jan. 2021, doi: 10.1109/TIE.2020.2965490.
[14]. A. Khaligh, J. Cao and Y. Lee," A Multiple-Input DC–DC Converter Topology," in IEEE Transactions on Power Electronics, vol. 24, no. 3, pp. 862-868, March 2009.
[15]. P. Prabhakaran and V. Agarwal," Novel Four-Port DC–DC Converter for Interfacing Solar PV–Fuel Cell Hybrid Sources with Low-Voltage Bipolar DC Microgrids," in IEEE Journal of Emerging and Selected Topics in Power Electronics, vol. 8, no. 2, pp. 1330-1340, June 2020, doi: 10.1109/JESTPE.2018.2885613.
[16]. Q. Tian, G. Zhou, M. Leng, G. Xu and X. Fan," Anon isolated Symmetric Bipolar Output Four-Port Converter Interfacing PV-Battery System," in IEEE Transactions on Power Electronics, vol. 35, no. 11, pp. 11731-11744, Nov. 2020, doi: 10.1109/TPEL.2020.2983113.
[17]. Jalilzadeh, T., Rostami, N., Babaei, E. and Hosseini, S.H, "Bidirectional multi-port dc–dc converter with low voltage stress on switches and diodes", IET Power Electronics, 13: 1593-1604.
[18]. F. Kardan, R. Alizadeh and M. R. Banaei," A New Three Input DC/DC Converter for Hybrid PV/FC/Battery Applications," in IEEE Journal of Emerging and Selected Topics in Power Electronics, vol. 5, no. 4, pp. 1771- 1778, Dec. 2017, doi: 10.1109/JESTPE.2017.2731816.
[19]. F. Akar, Y. Tavlasoglu, E. Ugur, B. Vural and I. Aksoy," A Bidirectional Nonisolated Multi-Input DC–DC Converter for Hybrid Energy Storage Systems in Electric Vehicles," in IEEE Transactions on Vehicular Technology, vol. 65, no. 10, pp. 7944-7955, Oct. 2016.
[20]. L. Chien, C. Chen, J. Chen and Y. Hsieh," Novel Three-Port Converter with High-Voltage Gain," in IEEE Transactions on Power Electronics, vol. 29, no. 9, pp. 4693-4703, Sept. 2014.
[21]. M. R. Al-Soeidat, H. Aljarajreh, H. A. Khawaldeh, D. D. -C. Lu and J. Zhu," A Reconfigurable Three-Port DC–DC Converter for Integrated PV-Battery System," in IEEE Journal of Emerging and Selected Topics in Power Electronics, vol. 8, no. 4, pp. 3423-3433, Dec. 2020, doi: 10.1109/JESTPE.2019.2941595.
[22]. B. R. Ravada, N. R. Tummuru and B. N. L. Ande," Photovoltaic-Wind and Hybrid Energy Storage Integrated Multi-Source Converter Configuration for DC Microgrid Applications," in IEEE Transactions on Sustainable Energy, vol. 12, no. 1, pp. 83-91, Jan. 2021, doi: 10.1109/TSTE.2020.2983985.
[23]. A. A. Saafan, V. Khadkikar, M. S. El Moursi and H. H. Zeineldin," A New Multiport DC-DC Converter for DC Microgrid Applications," 2021 IEEE Industry Applications Society Annual Meeting (IAS), 2021, pp. 1-7, doi: 10.1109/IAS48185.2021.9677403.
[24]. F. Nejabatkhah, S. Danyali, S. H. Hosseini, M. Sabahi and S. M. Niapour," Modeling and Control of a New Three-Input DC–DC Boost Converter for Hybrid PV/FC/Battery Power System," in IEEE Transactions on Power Electronics, vol. 27, no. 5, pp. 2309-2324, May 2012, doi: 10.1109/TPEL.2011.2172465.
[25]. J. J. Nedumgatt, K. B. Jayakrishnan, S. Umashankar, D. Vijayakumar and D. P. Kothari," Perturb and observe MPPT algorithm for solar PV systemsmodeling and simulation," 2011 Annual IEEE India Conference, 2011, pp. 1-6, doi: 10.1109/INDCON.2011.6139513.
[26]. X. Lu, K. Sun, J. M. Guerrero, J. C. Vasquez and L. Huang," DoubleQuadrant State-of-Charge-Based Droop Control Method for Distributed Energy Storage Systems in Autonomous DC Microgrids," in IEEE Transactions on Smart Grid, vol. 6, no. 1, pp. 147-157, Jan. 2015, doi: 10.1109/TSG.2014.2352342.
[27]. B. R. Ravada, N. R. Tummuru and B. N. L. Ande," PhotovoltaicWind and Hybrid Energy Storage Integrated Multisource Converter Configuration-Based Grid-Interactive Microgrid," in IEEE Transactions on Industrial Electronics, vol. 68, no. 5, pp. 4004-4013, May 2021, doi: 10.1109/TIE.2020.2984437.
[28]. R. Tonkoski, L. A. C. Lopes and T. H. M. El-Fouly," Coordinated Active Power Curtailment of Grid Connected PV Inverters for Overvoltage Prevention," in IEEE Transactions on Sustainable Energy, vol. 2, no. 2, pp. 139-147, April 2011, doi: 10.1109/TSTE.2010.2098483.